CJC Chinese Journal of Chemistry 中国化学 · An International Journal

For submission: https://mc.manuscriptcentral.com/cjoc
For published articles: https://onlinelibrary.wiley.com/journal/16147065

Chemistry Authors Up Close

Cite this paper: *Chin. J. Chem.* **2021**, *39*, 3188—3198. **DOI: 10.1002/cjoc.202100391**

Defect Luminescence Based Persistent Phosphors—From Controlled Synthesis to Bioapplications

Cailing Ji, Jie Tan, and Quan Yuan*

Institute of Chemical Biology and Nanomedicine, State Key Laboratory of Chemo/Biosensing and Chemometrics, College of Chemistry and Chemical Engineering, Hunan University, Changsha, Hunan 410082, China

What is the most favorite and original chemistry developed in your research group?
Synthesis and bioapplications of persistent phosphors.

How do you get into this specific field? Could you please share some experiences with our readers?
I got into chemistry related to biomedicine during my graduate student period. The research situation of luminescent nanomaterials in China has a strong effect on me, inspiring me to pursuit new luminescent nanomaterials and their applications.
We need have interest and concentrate on our research with passion. We are encouraged to work hard.

What is the most important personality for scientific research?
Curiosity and hard-working.

What are your hobbies? What's your favorite book(s)?
Shopping and reading books. My favorite books are novels, such as "The Three-Body Problem".

How do you keep balance between research and family?
I have two boys and it takes me much time to take care of them. I need to elevate my work efficiency and work hard. I also buy household service to save time.

Who influences you mostly in your life?
My father. He loves reading and writing. I know one need to have passion on something under my father's influence.

Quan Yuan

Professor, College of Chemistry and Chemical Engineering, Hunan University

E-mail: quanyuan@hnu.edu.cn

Homepage: http://quanyuan.whu.edu.cn/index.html

Birth: Feb. 6, 1982
Education: 2004 B.S. Wuhan University; 2009 Ph.D. Peking University
Experience:
2009–2011, Postdoctoral Fellow, Department of Chemistry, University of Florida;
2011–2017, Professor, College of Chemistry and Molecular Sciences, Wuhan University;
2017–present, Professor, College of Chemistry and Chemical Engineering, Hunan University
Awards:
2014 The National Science Fund for Excellent Young Scholars
2015 Chinese Chemical Society Prize for Young Scientists
2018 Nano Research Young Innovators Award
2019 The National Science Fund for Distinguished Young Scholars
Interests: Persistent phosphors; Biosensing and bioimaging

Keywords

Luminescence | Nanoparticles | Persistent phosphors | Synthesis design | Bioapplication

Abstract

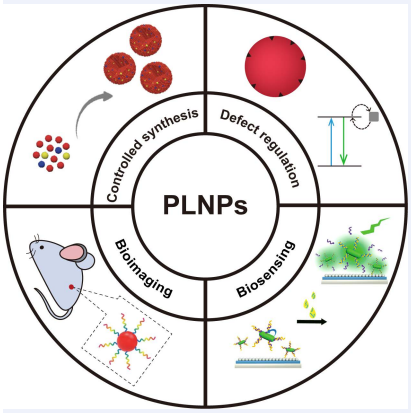

Persistent luminescence is an optical phenomenon where solid phosphors can store photoenergy in defects and release the energy by luminescence after stopping excitation. Due to the intriguing optical characteristics, the defect luminescence based persistent phosphors have attracted enormous attention in recent decades, especially in biomedical fields such as biosensing and bioimaging. Persistent luminescence nanoparticles (PLNPs) can effectively avoid the autofluorescence interference from complex samples or tissues, leading to significantly improved sensitivity in biological analysis. In this review, we summarized the methods to control the optical performance of PLNPs from the perspectives of controlled synthesis and defect regulation, and emphasized the close relationship between their optical performance and applications. We further provided a summary about a series of PLNPs nanoprobes designed by our group for biosensing and bioimaging. Our efforts, summarized in this review, will not only open a window for manipulating luminescence in PLNPs, but also further promote the application of PLNPs in biomedicine.

*E-mail: quanyuan@hnu.edu.cn

View HTML Article

Contents

1. Introduction

Persistent luminescence (PersL) refers to the optical phenomenon that luminescence lasts for seconds or even days after ceasing excitation.[1-4] PersL is originated from the crystal defects in solid phosphors (a substance that exhibits the phenomenon of luminescence), that is, a kind of defect luminescence.[5-7] Defects are the irregular arrangement of atoms in the crystal, such as vacancies and interstitials.[8-10] Under excitation, charge carriers are created and subsequently trapped by defects.[11-12] After excitation ceases, the trapped charge carriers can escape from the defects by thermal or other physical stimulations, and further recombine to generate the PersL.[11-12] Regulating the morphology and defects of the defect luminescence based persistent phosphors can control their optical properties, including the intensity, decay time and emission wavelength.[13-16] Generally, PersL intensity of persistent phosphors decreases with the increased particle diameter.[15] The intensity and decay time of PersL mainly depend on the depth of the trap levels in the bandgap. Phosphors with shallow traps mostly show a strong PersL intensity and a short lifetime. Whereas, deep traps usually produce a weak intensity and long-lasting luminescence.[17] In addition, ion doping tends to be accompanied by energy transfer, making it possible for the emission spectrum to change from blue to red.[18] Therefore, the defect luminescence based persistent phosphors can exhibit different optical properties by manipulating their morphology and defects. These various optical properties will endow persistent phosphors with the potential to meet different application requirements.[19-20]

The autofluorescence of biological chromophores usually interferes with conventional optical imaging.[21-22] Collecting the PersL signals after the short-lived autofluorescence disappears completely can effectively eliminate the autofluorescence interference.[23-24] Based on this property, defect luminescence based persistent phosphors have broad application prospects in biomedicine.[25-26] In biomedical applications, the optical properties of persistent phosphors will largely affect their performance in bioimaging and biosensing. Enhanced PersL intensity and prolonged decay time can effectively improve imaging sensitivity.[27-29] The long PersL decay time makes persistent luminescence materials suitable for long-term biological imaging.[30-31] In addition, there is a close relationship between the wavelength of PersL and the biological penetration depth. Tuning the wavelength to the near-infrared region can effectively improve the tissue penetration ability of the PersL signal.[23,25] By controlling the morphology and defects of persistent phosphors, the optical properties can be optimized to expand their applications in biomedicine.

In recent years, the significant progress in size and morphological control, PersL mechanism, and luminescence properties of persistent phosphors has greatly promoted their bioapplications.[32-33] As plenty of groundbreaking works have been reported, many reviews on persistent phosphor have also been published. At present, several excellent reviews emphasize the synthesis, functionalization and bioapplications of persistent phosphors. Qiu *et al.* made a comprehensive review on the synthesis methods, luminescence mechanisms, defect characterization techniques, material systems and applications of persistent phosphors.[13] Richard *et al.* systematically summarized the researches on persistent luminescent nanoparticles (PLNPs) with different matrixes for *in vitro* and *in vivo* imaging applications.[34] Yan *et al.* emphasized the surface engineering of PLNPs-based nanoprobes and their advances in bioapplications from biosensing/bioimaging to therapeutics.[32] Wang *et al.* provided a summary in the preparation of PLNPs and their applications in biosensing, bioimaging and cancer therapy.[33] Luo *et al.* reviewed the common surface modification methods and research progress of surface modified persistent phosphors in biosensing and bioimaging.[35] However, to our knowledge, the influence of morphology and defect regulation on the optical properties and bioapplications of persistent phosphors has rarely been reviewed. In this review, we present an overview of our efforts on defect luminescence based persistent phosphors from controlled synthesis methods, defect regulation to biomedical applications. In the first section, we describe the synthesis methods of PLNPs with different shapes. In the second section, we describe the relationship between defects and luminescence properties of PLNPs. In the last section, we summarize the applications of PLNPs in bioimaging and biosensing.

Cailing Ji received his B.S. degree in chemistry from Hunan University in 2019. She is currently pursuing her Ph.D. degree under the supervision of Prof. Quan Yuan at Hunan University. Her research interest is in developing functional nucleic acids for biomedical applications.

Jie Tan earned her Ph.D. degree from Zhejiang University in 2016. Then she joined the team of Prof. Weihong Tan in Hunan University as a postdoctoral fellow. Currently, she is an associate professor at Hunan University. Her main research interest is the design of chemically modified nucleic acids for biosensing.

2. Controlled Synthesis of PLNPs

The synthesis methods of PLNPs are of great significance to their microstructure and optical properties, and are also closely related to the application performance of PLNPs.[36] In recent years, the rapid development of biomedical field naturally puts forward more requirements on the morphology and luminescence properties of PLNPs.[37] This makes PLNPs with controllable morphology and size, excellent PersL properties, and effective surface functionalization become an emerging research trend. The conventional method for synthesizing PLNPs is the “top-down” approach such as a high temperature solid-state reaction. In this method, grinding is required to break down the bulk rough grains into nanoparticles.[38] However, PLNPs prepared by the top-down method usually show insignificant surface modification, poor dispersion, and heterogeneous size and shape distribution.[13] Such shortcomings affect the PersL properties of PLNPs, further hindering their biomedical applications. To prepare PLNPs with controlled properties for biomedical applications, our group and oth-

er researchers have pioneered the bottom-up methods for PLNPs synthesis.[39-41]

2.1. Hydrothermal/solvothermal method

Hydrothermal/Solvothermal method refers to a synthetic method, where the precursor solution is reacted in a closed system at a certain temperature and pressure.[42] Hydrothermal/solvothermal method has the advantages of low synthesis temperature, mild conditions and relatively stable system.[41-42] This method, therefore, represents a high-efficiency and energy-saving synthesis method for nanomaterials. The controllable reaction parameters can enable the synthesis of PLNPs with easy dispersion and surface functionalization.[13] Additionally, the properties of the PLNPs can be easily regulated by changing the reaction parameters.[38] Our group has developed several solvothermal methods for the controlled synthesis of PLNPs.

As illustrated in the synthesis route outlined in Figure 1a, we controlled the chemical composition of PLNPs and prepared a series of $Zn_{1+x}Ga_{2-2x}Ge_xO_4$:Cr ($0 \le x \le 0.5$, ZGGO:Cr) nanoparticles with tunable properties.[43] Transmission electron microscopy (TEM) images show that these ZGGO:Cr nanoparticles are well-dispersed and have uniform shape and size (Figure 1b). The size of ZGGO:Cr nanoparticles gradually increases from about 7 nm to around 80 nm as the value of *x* increases. The PersL decay images in ZGGO:Cr nanoparticles (Figure 1c) further shows that the ZGGO:Cr nanoparticles are all activated by an orange LED, and strong PersL can be detected after the cessation of excitation. With the increase of *x* from 0 to 0.5, the decay time and PersL intensity primarily increase and then decrease. It is worth noting that the PersL of ZGGO:Cr nanoparticles with $x = 0.2$ is still strong even after 10 h of decay, indicating their potential prospects for long-term bioimaging.

We also prepared a series of Zn_2GeO_4:Mn (ZGO:Mn) PLNPs with different sizes and PersL properties by controlling the pH of the hydrothermal reaction system.[44] As shown in Figure 1d, ZGO:Mn PLNPs are well-dispersed with typical rod shape. By increasing the pH of the reaction system from 6.0 to 7.5, the length of the ZGO:Mn PLNPs decreases rapidly from about 900 nm to 60 nm. The length of the nanorods further increases to nearly 80 nm when the pH increases to 9.5. The luminescence images of ZGO:Mn PLNPs dispersion under excitation (Figure 1e) present that the luminescence of the ZGO:Mn PLNPs changes gradually from blue to green with the increase of pH. This can be attributed to the gradual increase of Mn^{2+} emission and decrease of defect luminescence. After the removal of excitation, ZGO:Mn PLNPs display strong PersL and adjustable luminescence color (Figure 1f). Additionally, we also realized regulating the size and PersL properties of $Zn_{1.5}GaGe_{0.5}O_4$:Cr PLNPs by the similar method.[42] These results confirm that the properties of PLNPs can be well tuned by simply changing the reaction parameters of the hydrothermal system.

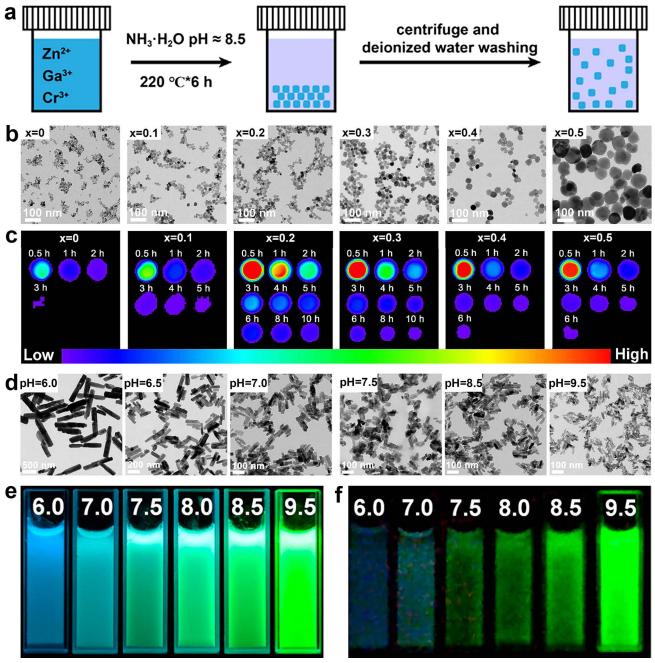

Figure 1 (a) Schematic illustration of the synthesis of $Zn_{1+x}Ga_{2-2x}Ge_xO_4$:Cr ($0 \le x \le 0.5$) PLNPs by the hydrothermal method. (b) TEM images and (c) PersL decay images of $Zn_{1+x}Ga_{2-2x}Ge_xO_4$:Cr ($0 \le x \le 0.5$) PLNPs. Reprinted with permission.[43] (d) TEM images, (e) photoluminescence images and (f) PersL images of the Zn_2GeO_4:Mn PLNPs prepared at different pH values. Reprinted with permission.[44]

Based on hydrothermal/solvothermal method, we synthesized ZGO:Mn PLNPs with different morphologies by a molecular coordination method.[45] Specifically, organic amines serve as a structure-directing reagent. Due to the difference in the number of amino groups, amine ligands will exhibit different coordination capabilities. By introducing ethylenediamine, butanediamine, and diethylenetriamine, the morphology of ZGO:Mn changes from nanorods to dumbbells, and finally to spherical shapes with the increase of the amino groups in the ligand (Figure 2a). At the same time, the diameter of the spikes that make up the dendrites gradually decreases. Among them, by using triethylenetetramine as the ligand, we obtained uniform ZGO:Mn flower-like dendrites with dense and sharp spikes. The element mapping image and EDX analysis results show the uniform distribution of Zn, Ge, O and Mn in the crystal (Figure 2b). The phosphorescence spectrum indicates that ZGO:Mn PLNPs have strong long-lived emission (Figure 2c). The PersL decay images show that ZGO:Mn PLNPs exhibit strong PersL and long decay time (Figure 2d). The above observations demonstrate that the morphology of PLNPs can be well-tuned by changing the coordination ability of the ligand in the hydrothermal reaction system.

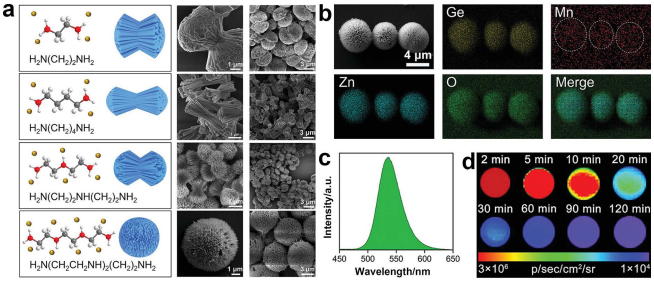

Figure 2 (a) The schematic illustration, and SEM images of Zn_2GeO_4:Mn persistent phosphors synthesized with amine ligands with different coordination abilities. (b) The element mapping images of the Zn_2GeO_4:Mn radiated dendrites. (c) The phosphorescence spectrum of Zn_2GeO_4:Mn PLNPs. (d) The PersL decay images of Zn_2GeO_4:Mn PLNPs. Reprinted with permission.[45]

Furthermore, we developed a biphase solution chemical reaction system to directly synthesize one-dimensional ZGO:Mn PLNPs.[46] We showed that the phase, morphology and PersL properties of PLNPs can be effectively controlled by adjusting the hydrothermal reaction time. In addition, doping can fine-tune the PersL intensity and the decay time of ZGO:Mn PLNPs. We believe that these unique nanostructured PLNPs prepared by this chemical method without solid-state reactions will facilitate the development of imaging optical devices.

2.2. Thermal decomposition method

Thermal decomposition method refers to the preparation of

nanocrystals by thermally decomposing the precursor in high-boiling solvent.[47-48] It is one of the best methods for synthesizing stable and small monodisperse nanoparticles with controllable morphology and size.[49-50] By changing the precursor/surfactant ratio, reaction temperature, reaction time and aging period, the size and morphology of the nanoparticles can be precisely controlled.[51] Due to these advantages, nanomaterials are widely synthesized by thermal decomposition method, including upconversion nanoparticles, magnetic nanoparticles and rare earth oxide nanocrystals.[52-54] Recently, thermal decomposition method has been used for the synthesis of PLNPs by our group.

We reported a thermal decomposition method based on metal acetylacetonates for controlled synthesis of PLNPs with sub-5 nm size (Figure 3a).[55] In this method, metal acetylacetonates are used as the precursors due to their proper decomposition speed during thermal reactions. Oleylamine is used as the solvent and the stabilizer to avoid the aggregation of the nanocrystals. With this approach, we prepared the $ZnGa_2O_4$:Cr (ZGO: Cr) PLNPs. Moreover, the luminescence properties of ZGO:Cr can be enhanced by doping ions such as Al^{3+} or Sc^{2+}. As shown in Figure 3b, Al^{3+}-doped ZGO:Cr (ZGO:Al,Cr) PLNPs display uniform morphology and good dispersion. Size distribution curve indicates that the average size of ZGO:Al,Cr PLNPs is about 5 nm (Figure 3c). With the Al^{3+} concentration increased from 0 to 0.1%, the phosphorescence intensity and PersL intensity of the ZGO:Al,Cr gradually increase (Figures 3d—3e). Moreover, we extend the thermal decomposition method to other persistent phosphor systems, including sulfide and fluoride. Specifically, we have synthesized ZnS:Cr and CaF_2 by this method. The PersL in the ZnS:Cr PLNPs and CaF_2 PLNPs can last for more than 30 min and 1 h, respectively. Overall, the thermal decomposition method can be used to prepare the PLNPs, and the PersL properties of the obtained PLNPs can be well controlled by methods such as ion doping.

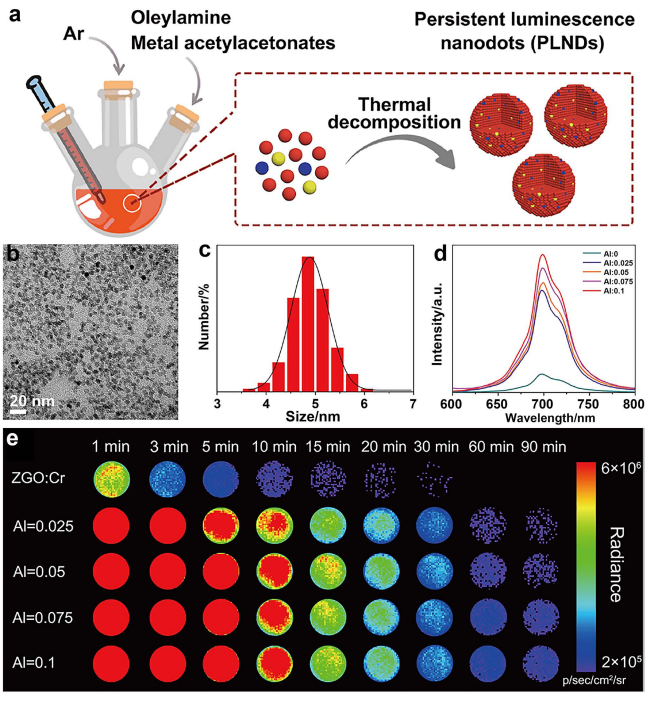

Figure 3 (a) Schematic illustration of the controlled synthesis of PLNPs by a thermal decomposition method. (b) TEM image, (c) size distribution, (d) phosphorescence spectra, and (e) PersL decay images of the ZGO:Al,Cr PLNPs. Reprinted with permission.[55]

Together, to acquire the optimal solution between morphology/size and PersL performance, the synthesis methods have been studied and improved from several aspects. Compared to the "top-down" approaches, the "bottom-up" methods have significant advantages in the morphology and uniformity control of the preparation of PLNPs.[13,39-41] By changing the reaction conditions such as temperature and pH, PLNPs with different morphologies and sizes can be obtained, and the PersL properties of PLNPs can also be optimized. Controllable synthesis of PLNPs is a key factor affecting their biomedical applications.[56] Although great progress has been achieved, the preparation of PLNPs by the "bottom-up" methods is still in the research stage, and the reported approaches only partially improve the performance of PLNPs.[30,38,57] So far, there is no general synthesis technology that can accurately control the morphology/size and PersL properties of PLNPs at the same time to meet the different needs of biomedical applications. Therefore, in the future, existing synthesis methods should be further improved or new synthesis methods need to be developed to simultaneously optimize the morphology, particle size and PersL properties of PLNPs.

3. Defect Regulation

The intensity and duration of PersL directly affect the application performance of PLNPs in biomedicine.[58] During the *in vivo* imaging, the PersL intensity of PLNPs decreases over time, resulting in a declining imaging sensitivity.[59] Most PLNPs need to be activated by ultraviolet (UV) irradiation. Due to the limited tissue penetration of UV, PLNPs cannot be effectively reactivated by UV light.[60] Therefore, regulating the emission wavelength of PLNPs from UV to visible, or even near-infrared, is beneficial for expanding their bioapplications. The researches on the structure and PersL mechanism of PLNPs provides guidance for the design of PLNPs that are suitable for specific bioapplications. The overall mechanism of PersL is now recognized to be involved in the formation of defects in phosphors.[7,12] With the increased number of defects in the phosphor, the stored energy increases, thereby PersL can be enhanced. Whereas, high-density defects will cause a concentration quenching effect, resulting in a weakening of PersL.[43,61] Modulating the defects in persistent phosphors is not only helpful to study the mechanism of PersL, but also can realize the regulation of the PersL intensity and decay time.

3.1. Hetero-valence ion doping

By doping host lattices with ions that have different valence from the host ions, hetero-valence ion doping can serve as an effective strategy to effectively introduce charged defects into the host lattice.[62] The hetero-valence doped ions usually act as luminescence centers or energy transfer mediators to affect the luminescence characteristics of persistent phosphors.[62-63]

By hetero-valence ion doping strategy, we prepared $Zn(Ga_{1-x}Zn_x)(Ga_{1-x}Ge_x)O_4$:Cr PLNPs by doping Ge^{4+} into $ZnGa_2O_4$:Cr (ZGO:Cr) to investigate the relationship between defects and PersL properties.[64] As shown in Figure 4a, the $Zn(Ga_{1-x}Zn_x)(Ga_{1-x}Ge_x)O_4$:Cr PLNPs present a broad emission ranging from 650—750 nm in the photoluminescence spectra. The peak near 715 nm is the Stokes phonon sideband line, indicating that Cr^{3+} occupies the ideal octahedral position. Previous studies have shown that the PersL of ZGO:Cr is mainly contributed by the N2 line emission.[12] Obviously, the N2 line turns stronger with increasing the doped ratio of Ge^{4+}. The PersL decay curves of $Zn(Ga_{1-x}Zn_x)(Ga_{1-x}Ge_x)O_4$:Cr PLNPs are presented in Figure 4b. Compared with undoped ZGO:Cr, the luminescence intensity of doped persistent luminescence materials is significantly enhanced, and the intensity increases with the addition of doped Ge^{4+}. The above results clearly illustrate that hetero-valence doping of Ge^{4+} alters the local structure of Cr^{3+}, affecting the luminescent properties of the PLNPs.

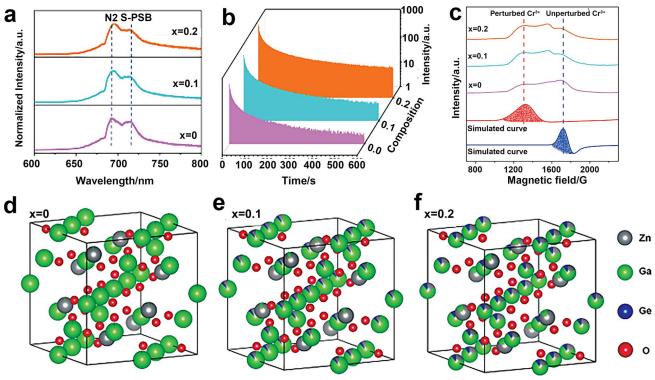

Figure 4 (a) Photoluminescence spectra, (b) PersL decay curves and (c) EPR spectra of $Zn(Ga_{1-x}Zn_x)(Ga_{1-x}Ge_x)O_4$:Cr PLNPs. N2: N2 zero photon line. S-PSB: Stokes phonon sideband line. Schematic illustration of the crystal structure of (d) $ZnGa_2O_4$:Cr, (e) $Zn_{1.1}Ga_{1.8}Ge_{0.1}O_4$:Cr and (f) $Zn_{1.2}Ga_{1.6}Ge_{0.2}O_4$:Cr. Reprinted with permission.[64]

Further, we investigated the number of charge defects near Cr^{3+} in $Zn(Ga_{1-x}Zn_x)(Ga_{1-x}Ge_x)O_4$:Cr using low temperature electron paramagnetic resonance (EPR). Then we simulated the charge defects near disturbed and undisturbed Cr^{3+} in octahedral locations, respectively. The absorption band of perturbed Cr^{3+} is weaker than that of unperturbed Cr^{3+} in ZGO:Cr (Figure 4c). With the increase of doped Ge^{4+}, the absorption band of perturbed Cr^{3+} gradually increases, while that of undisturbed Cr^{3+} becomes weaker. These results show that the perturbation of Cr^{3+} content in $Zn(Ga_{1-x}Zn_x)(Ga_{1-x}Ge_x)O_4$:Cr increases significantly with the hetero-valent doping of Ge^{4+}. This may be due to the increase of charged defects in the lattice. As shown in Table 1, the number of positively charged defects Ge°_{Ga}, Ga°_{Zn} and negatively charged defects $Zn^{'}_{Ga}$ increases significantly with the increase of the doping amount of Ge^{4+}. The observation reveals that a large number of charge defects have been introduced into $Zn(Ga_{1-x}Zn_x)(Ga_{1-x}Ge_x)O_4$:Cr by doping hetero-valence ions. We also studied the crystal structure of $Zn(Ga_{1-x}Zn_x)(Ga_{1-x}Ge_x)O_4$:Cr *via* Rietveld refinement. Compared with ZGO:Cr (Figure 4d), all of the doped Ge^{4+} ion enters the octahedral sites in $Zn_{1.1}Ga_{1.8}Ge_{0.1}O_4$:Cr (Figure 4e) and $Zn_{1.2}Ga_{1.6}Ge_{0.2}O_4$:Cr (Figure 4f). Specifically, the amount of Ga^{3+} ions at tetrahedral site and Zn^{2+} ions at octahedral site in $Zn_{1.2}Ga_{1.6}Ge_{0.2}O_4$:Cr are much higher than that at $Zn_{1.1}Ga_{1.8}Ge_{0.1}O_4$:Cr. Together, ion doping can introduce defects into the PLNPs and thus achieve the regulating of their PersL properties.

Table 1 Charge defects in $Zn(Ga_{1-x}Zn_x)(Ga_{1-x}Ge_x)O_4$:Cr. Reprinted with permission.[64]

Composition (x)	Ge°_{Ga}	$Zn^{'}_{Ga}$	Ga°_{Zn}
0	0	0.03	0.03
0.1	0.1	0.18	0.08
0.2	0.2	0.38	0.18

3.2. Surface defects passivation

Many studies have reported the relationship between defects and PersL, whereas the influence of surface defects on PersL remains unclear.[8-12] Surface defects are the most commonly encountered defects for nanomaterials.[65-67] A large number of exposed atoms on the surface of nanomaterials lead to the production of surface defects for the balance of charge[68]. Surface defects are widespread on the surface of nanomaterials and can affect their luminescence performance.[69] Our group investigated the influence of surface defects on the PersL of PLNPs.

Taking the classic zinc gallogermanate (ZGGO:Cr) PLNPs as the model, we investigated the relationship between surface defects and PersL.[61] By utilizing the surface coating strategy to passivate the surface defects, we prepared two core-shell structured PLNPs, $Zn_{1.2}Ga_{1.6}Ge_{0.2}O_4$:Cr@$ZnGaO_4$ (ZGGO:Cr@ZGO) and $Zn_{1.2}Ga_{1.6}Ge_{0.2}O_4$:Cr@$SiO_2$ (ZGGO:Cr@SiO_2) (Figure 5a). TEM images show that the synthesized ZGGO:Cr@ZGO exhibits a uniform quasi-spherical shape with an average diameter of about 15 nm (Figure 5b). High-angle annular dark-field scanning transmission electron microscopy (HAADF-STEM) image clearly presents the core-shell structure of ZGGO:Cr@ZGO, manifesting the successful epitaxial growth of the $ZnGaO_4$ shell (Figure 5c). ZGGO:Cr@SiO_2 also shows a uniform quasi-spherical shape (Figure 5d) and a clear core-shell structure (Figure 5e). Further, we investigated the luminescence properties of ZGGO:Cr@ZGO and ZGGO:Cr@SiO_2. The luminescence decay curve reveals that ZGGO:Cr@ZGO and ZGGO:Cr@SiO_2 have stronger PersL intensity than ZGGO:Cr (Figure 5f). The corresponding luminescence decay image further proves that ZGGO:Cr@ZGO and ZGGO:Cr@SiO_2 exhibit stronger PersL intensity and longer decay time than uncoated ZGGO:Cr (Figure 5g). These observations demonstrated that surface defects quench the PersL in PLNPs. Surface defect passivation can effectively enhance the PersL intensity and prolong the PersL time in PLNPs.

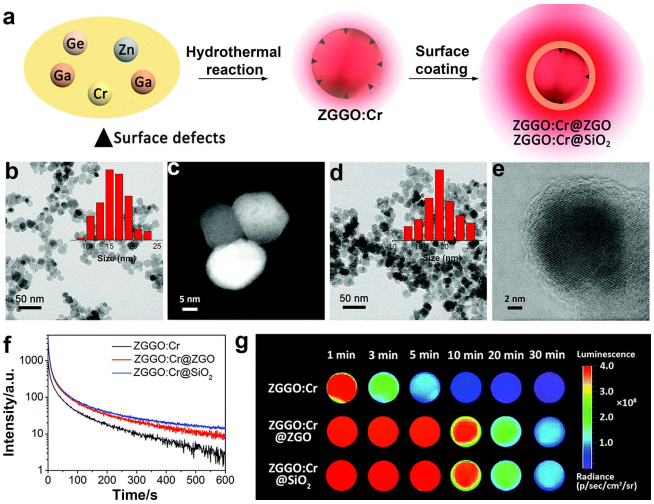

Figure 5 (a) Schematic illustration of surface defects passivation of PLNPs by a surface coating strategy. (b) TEM image and corresponding size distribution of the ZGGO:Cr@ZGO PLNPs. (c) HAADF-STE image of the ZGGO:Cr@ZGO PLNPs. (d) TEM image and corresponding size distribution of the ZGGO:Cr@SiO_2 PLNPs. (e) HAADF-STE image of the ZGGO:Cr@SiO_2 PLNPs. (f) The luminescence decay curve and (g) corresponding luminescence decay images of ZGGO:Cr, ZGGO:Cr@ZGO and ZGGO:Cr@SiO_2 PLNPs. Reprinted with permission.[61]

The excitation and emission characteristics of PersL are critical factors affecting the biomedical applications of PLNPs. To make full use of PLNPs for *in vivo* biosensing and bioimaging, the main strategy is to modulate trap types, depths and concentrations by changing the crystal structure of the host material.[20,70] At present, researchers mainly use rare earth ion doping and other methods to achieve defect regulation of PLNPs.[71-72] All in all, defect plays a crucial role in PersL. However, the current understanding of the defect characteristics of PLNPs is not comprehensive enough, and the understanding of how defects participate in the PersL process is not deep enough. The relationship between defects and PersL should be further studied in the future, thereby optimizing effectively the bioapplication performance of PLNPs *via* defect regulation.

4. Biomedical Applications

In the past few decades, due to their significant advantages of high sensitivity, non-invasive and time-efficient, optical sensing and imaging technologies have become indispensable tools in the biomedicine and life sciences.[73-74] So far, a variety of advanced fluorescent probes, such as fluorescent dyes, metal complexes, upconversion nanoparticles, and persistent phosphors, have been developed and successfully applied in biomedicine.[75-76] Among these, persistent phosphors show unprecedented advantages in bioimaging and biosensing due to their unique ability to eliminate the interference of autofluorescence from biological samples.[23-26] The optical properties such as the PersL intensity and lifetime of phosphors will inevitably affect biomedical applications.[19-20,23] Regulating the morphology and defects can further optimize the luminescence properties of PLNPs, making them better applied in biomedicine. Our group has successfully applied the optimized PLNPs to fingerprint imaging and bioimaging, and further realized the detection of clinical samples, such as human serum and urine.[43-44,77-79]

4.1. Fingerprint imaging

Fingerprints contain a large amount of information such as friction ridge patterns and the metabolism of the donors, which are widely applied in forensic investigation and access control.[80] Latent fingerprints are the most common form of fingerprints.[81] For fingerprints on substrates that can produce background fluorescence, latent fingerprint images are usually masked, which severely reduces sensitivity and resolution of current imaging method.[82] Persistent phosphors can effectively avoid background fluorescence through collecting the PersL signal after the short-lived background fluorescence has decayed.[23-24] Accordingly, persistent phosphors hold the potential to be an ideal choice for latent fingerprint imaging.

We reported a strategy that uses PLNPs to realize background-free latent fingerprint imaging (Figure 6a).[78] Acting as labeling agents for latent fingerprint detection, persistent luminescence materials functionalized with carboxyl groups can be linked to fingerprint by reacting with the amino groups in fingerprint ridges. Under excitation, the substrate exhibits strong background fluorescence, leading to the seriously blurred fingerprint image. After excitation ceases, the background fluorescence decays rapidly, while the PLNPs remain luminescent, presenting a clear fingerprint image. The ZGO:Ga,Mn-COOH nanoparticles were utilized to mark the fingerprints on a poker card and a soft drink can to investigate imaging capability. As shown in Figure 6b and Figure 6c, the ZGO:Ga,Mn-COOH effectively avoided the interference of background fluorescence, and bright fingerprint images with clear ridges can be observed. Notably, the high-quality fingerprint images make it possible to visualize specific details. Under higher magnification, the detailed information of the fingerprint such as termination, bifurcation, whorl, and lake, can be clearly confirmed. The above results prove convincingly that PLNPs can effectively eliminate background fluorescence interference and are valuable in latent fingerprint imaging.

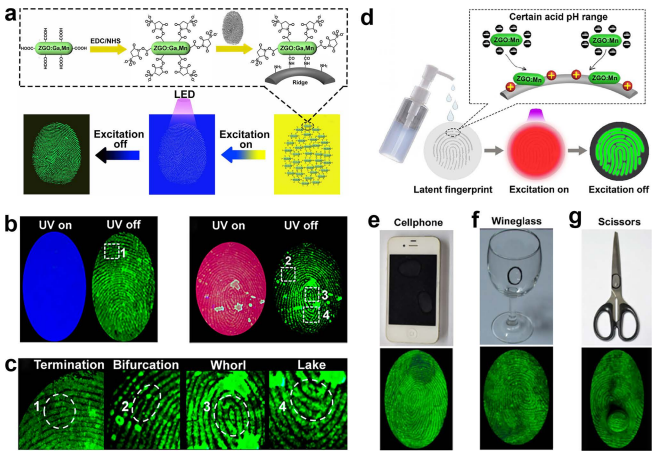

Figure 6 (a) Schematic Illustration of background-free latent fingerprint imaging strategy with ZGO:Ga,Mn-COOH PLNPs. (b) Photograph of a treated fingerprint on a poker card (left) and a soft drink can (right) under excitation and after excitation ceased. (c) Specific details of (b). Reprinted with permission.[78] (d) Schematic illustration of the easy-to-perform strategy for background-free latent fingerprint imaging with ZGO:Mn-COOH PLNPs. Photographs and luminescent images of marked fingerprints on (e) a cellphone, (f) a wineglass, and (g) scissors. Reprinted with permission.[83]

We further established a more easy-to-perform strategy for background-free fingerprint imaging based on electrostatic interaction.[83] As shown in Figure 6d, fingerprint imaging is realized by simply dropping the acidic Zn_2GeO_4:Mn-COOH (ZGO:Mn-COOH) colloidal dispersion stored in a portable spray bottle on the latent fingerprints. In a certain acidic pH range, ZGO:Mn-COOH PLNPs are negatively charged, whereas the proteins and amino acids in the latent fingerprints are positively charged, resulting in ZGO:Mn-COOH PLNPs binding to ridges in latent fingerprints by electrostatic interaction. Under excitation, the image of latent fingerprints is blurry. After the excitation is switched off, the ZGO:Mn-COOH PLNPs remain luminescent to show a clear fingerprint image. Without destructive operations, ZGO:Mn-COOH PLNPs can specifically bind to latent fingerprints only by adjusting the pH of the ZGO:Mn-COOH colloidal dispersion. Importantly, the acidic ZGO:Mn-COOH colloidal dispersion can be stored in a portable spray bottle for on-site detection. We used this imaging method to mark fingerprints on a mobile phone display screen, a wineglass, and scissors (Figure 6e). All the obtained fingerprints can display clearly visible fingerprint details. Collectively, ZGO:Mn-COOH nanoparticles display great versatility for removing background interference, suggesting their capabilities in potential areas such as criminal investigation and anti-counterfeiting authentication.

4.2. Bioimaging

Optical bioimaging is an indispensable technology in modern biomedicine.[84] It has the advantages of high sensitivity, non-invasiveness, and easy operation.[85] Despite the many advantages, this technique is susceptible to interference from tissue autofluorescence.[21-24] Studies have found that persistent phosphors can effectively eliminate autofluorescence interference in bioimaging due to the long decay time of PersL.[23-24] In a proof of concept study, we used $Zn_{1.2}Ga_{1.6}Ge_{0.2}O_4$:Cr (ZGGO:Cr) PLNPs for autofluorescence-free bioimaging.[43] After autofluorescence attenuates completely, the interference of autofluorescence can be avoided by gathering the PersL signal of ZGGO:Cr nanoparticles. As demonstrated in Figure 7a, ZGGO:Cr nanoparticles injected into mice were activated *in vivo*. The strong autofluorescence in mice under excitation leads to the poor imaging sensitivity and low signal-to-noise ratio. The autofluorescence disappears rapidly after the stoppage of excitation, but the remaining PersL signal eliminates the interference of autofluorescence. Moreover, ZGGO: Cr, cyanine derivative dye and Ag_2Se quantum dots were subcutaneously injected into mice for bioimaging (Figure 7b). Obviously, the PersL signal of ZGGO:Cr nanoparticles (left panel) is clear without autofluorescence interference. On the contrary, cyanine derivative dye (middle panel) and Ag_2Se quantum dots (right panel) injected mice both are observed with strong autofluorescence, making it difficult to distinguish the emission signal of cyanine derivative dye and Ag_2Se quantum dots. The comparison demonstrates the potent ability of ZGGO:Cr nanoparticles in eliminating autofluorescence interference.

We further developed the ZGGO:Cr PLNPs functionalized with aptamer (ZGGO:Cr-Apt) for tumor-targeting imaging *in vivo*. After injection, an obvious Persl signal is observed at tumor sites in 10 min and the peak signal intensity is reached at 1 h (Figure 7c). It is worth noting that luminescence signal at tumor sites is still visible obviously at 5 h. Subsequently, the mice injected with ZGGO:Cr-Apt were dissected and *in vitro* images of tumor and various organs are obtained in Figure 7c. These observations prove powerfully that persistent phosphors are ideal for long-term free-autofluorescence targeted biological imaging and hold broad prospects in cancer diagnosis.

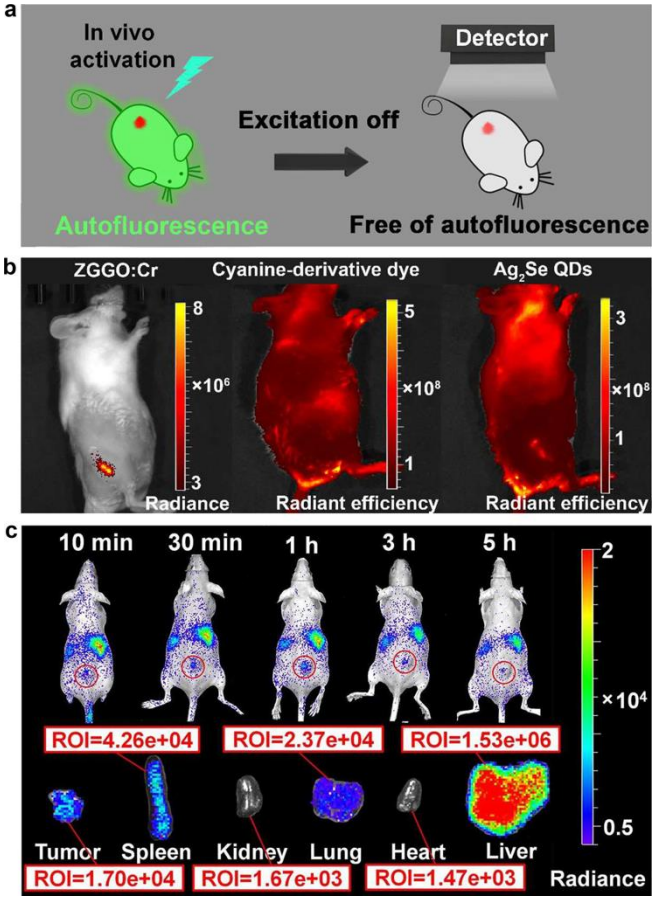

Figure 7 (a) Schematic illustration of the elimination of autofluorescence interference by ZGGO:Cr nanoparticles. (b) *In vivo* imaging of mice after different treatments. (c) *In vivo* and *in vitro* luminescent images of mice after injection of ZGGO:Cr-Apt nanoparticles. Reprinted with permission.[43]

4.3. Biosensing

The detection of biomarkers in complex samples plays an important role in early diagnosis and treatment evaluation.[86] At present, fluorescence analysis has been widely used in biosensing due to its high selectivity and sensitivity.[87] However, complex biological samples contain a variety of biomolecules, resulting in strong background fluorescence interference.[88-89] Phosphors with long lifetime luminescence have the potential to eliminate autofluorescence in complex samples due to their unique optical properties.[23-24] Therefore, we studied the application of our developed PLNPs in biosensing.

The ZGO:Mn PLNPs functionalized with lysozyme-binding aptamer (ZGO:Mn-LBA) were prepared for detection of lysozyme in serum. The photoluminescence and PersL spectra of the mixed solution were obtained by adding ZGO:Mn-LBA into serum (Figure 8a).[44] The curve shows that strong fluorescence appears in 400—600 nm in photoluminescence spectra and the autofluorescence seriously covers the luminescence signal of ZGO:Mn-LBA at 536 nm. The phosphorescence curve demonstrates that autofluorescence of serum disappears completely after taking off excitation. The unique long-lived PersL signal of ZGO:Mn-LBA was obtained in the process of detection. The spectra clearly indicate that ZGO:Mn-LBA can effectively eliminate the interference of serum autofluorescence. We further analyzed the response of the biosensing probe to lysozyme, and measured the phosphorescence curve in the presence of lysozyme with different concentrations (Figure 8b). The spectra reveal that the addition of lysozyme resulted in the effective recovery of the PersL of the biosensing probe. The above results clearly indicate that ZGO:Mn-LBA can effectively eliminate the interference of serum autofluorescence, exhibiting excellent biosensing performance.

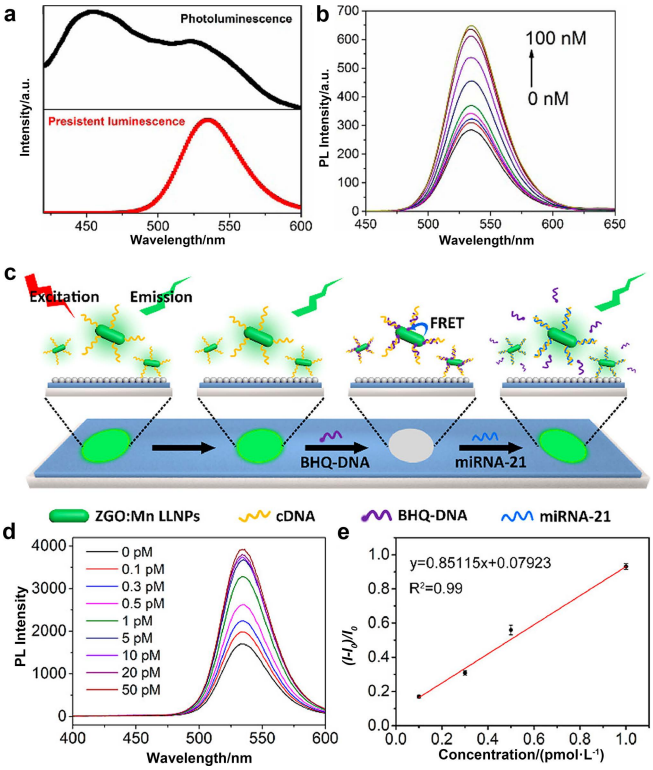

Figure 8 (a) Photoluminescence and PersL spectra of the mixed solution of ZGO:Mn-LBA and human serum. (b) The phosphorescence curve of ZGO:Mn-LBA in the presence of lysozyme with different concentrations. (c) Schematic illustration of the detection of bladder cancer-related miRNA-21 in urine by the portable biochip. (d) The recovered long-lifetime luminescence of the portable biochip in the presence of different concentrations of miRNA-21. (e) The quantitative analysis of (d). Reprinted with permission.[79]

We further developed a portable biochip for the detection of bladder cancer-related miRNA-21 in urine (Figure 8c).[79] The ZGO:Mn PLNPs are modified with cDNAs that are completely complementary to miRNA-21, followed by being hybridized partially with black-hole-quencher-labeled DNAs (BHQ-DNAs). The fluorescence resonance energy transfer between ZGO:Mn and BHQ dyes can quench the PersL. When miRNA-21 is added, the longer-sequence miRNA-21 is more competitive with cDNAs, causing the separation of BHQ-DNAs from cDNAs and the fluorescence recovery of ZGO:Mn PLNPs. After the excitation is turned off, the biochip can remain luminescent. Whereas the autofluorescence of the co-excited biomolecules decays rapidly, signifi-

cantly reducing the background signal. With the increased amount of miRNA-21, the intensity of long-lifetime luminescence gradually recovered (Figure 8d). The quantitative analysis in Figure 6e illustrates a linear relationship between the PersL intensity and the concentration of target miRNA-21 ranging from 0.1—1 pmol/L. According to the $3s/\sigma$ criterion (s, the standard deviation of 11 blank samples; σ, the slope of the linear working curve), the limit of detection (LOD) of miRNA-21 is calculated as 26.3 fmol/L. These results indicate that the biochip presents high sensitivity and low background for the analysis of miRNA in urine samples.

Furthermore, we combined immunebiosensors, signal-amplification biochips and Python image algorithms to construct an intelligent diagnostic system for detecting bacteria in urine samples (Figure 9a).[77] Based on antibody-antigen recognition, antipathogenic bacteria antibody functionalized ZGO:Mn PLNPs are used to specifically bind and capture target bacteria to form immune complexes. Subsequently, the photonic crystals integrated in the biochip enhance PersL signal. Finally, a machine vision algorithm is used to analyze the PersL signal and convert it into a digital signal. Luminescence spectra showed that in the presence of *Escherichia coli* (*E. coli*) or *Staphylococcus aureus*, a strong emission band peak is observed, while no obvious emission band is found in negative samples (Figures 9b,c). This indicates that the bacteria specifically bind to ZGO:Mn PLNPs modified by antibodies. Positive samples and negative samples are placed on the PC-based biochip, respectively, and then the collected luminescence images are processed by the image algorithm (Figure 9d). After calculation, positive samples show a higher luminance value than negative samples (Figure 9e). These results indicate that the intelligent system can be used for rapid bacterial detection based on bacteria-specific labeled PLNPs. Reasonably designed PersL bioprobes make it possible to detect a variety of significant

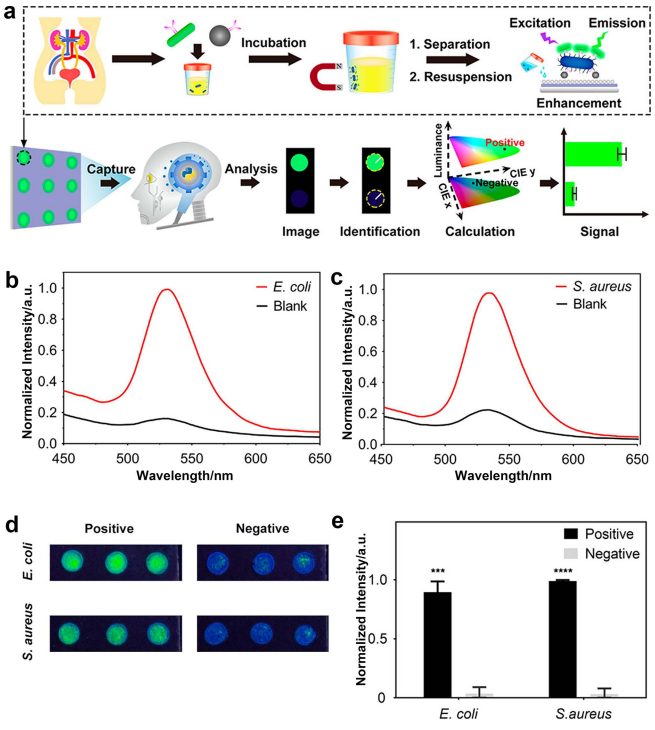

Figure 9 (a) Illustration of the intelligent diagnostic system combining immunebiosensors, signal-amplification biochips and Python image algorithms. Luminescence spectra of immunocomplexes in the presence of *Escherichia coli* (b) or *Staphylococcus aureus* (c). (d) Images of positive and negative samples placed on a PC biochip respectively. (e) Normalized luminance values of positive samples and negative samples. Reprinted with permission.[77]

biomarkers and have great potential in the fields of medical diagnosis and health assessment.

Compared with traditional optical probes, PLNPs can efficiently eliminate autofluorescence, making them more suitable for a wide range of bioapplications.[90-91] However, the applications of PLNPs in biomedicine such as biosensing and bioimaging are still in the developmental stage. In general, skin, water, and deoxyhemoglobin in living tissues are strong UV-visible absorbents.[92] Most PLNPs require UV excitation, inevitably causing serious damage to the organism.[93] Meanwhile, the penetration ability of UV light to tissues is weak.[94] More types of PLNPs suitable for long-term and deep tissue bioimaging need to be developed, such as the PLNPs that can be directly charged by near infrared light. In addition, PLNPs imaging is highly sensitive, but it cannot provide all the information needed for disease diagnosis.[19] Therefore, it is essential to combine PersL imaging with other imaging modalities to present more comprehensive and reliable information for disease diagnosis.

5. Conclusions

The defect luminescence based persistent phosphors have attracted a lot of attention in biomedicine due to its sustainable luminescence without external continuous illumination. In this review, we discussed the mechanism of how the morphology and defects of PLNPs affect their PersL performance, and summarized our recent works in biomedical applications of PLNPs. Our research attempts to confer various optical properties on PLNPs by controlled synthesis and defect regulation, and further expand the application of PLNP nanoprobes in bioimaging and biosensing. A variety of PLNPs engineered nanoprobes have been developed for clinical complex samples detection and tumor targeted imaging. Although great progress has been made based on PLNPs, there are still many problems need to be solved: (1) PLNPs with uniform size, strong PersL intensity and long decay time are of great significance in biomedical applications. There is currently a lack of novel general synthesis methods to control the morphology and optical properties to obtain such high-quality PLNPs. (2) The excitation range of most traditional PLNPs is in the ultraviolet region. This kind of high-energy excitation light will inevitably cause certain damage to the organism and has shallow tissue penetration. (3) Currently, PLNP-based nanoprobes are mainly used for tumor imaging, diagnosis and treatment. PLNPs can be vigorously tapped into the diagnosis and treatment potential of serious diseases such as cardiovascular and cerebrovascular diseases. In short, PLNPs have demonstrated unprecedented advantages in biosensing and bioimaging, playing a pivotal position in the future of life science.

Acknowledgement

This work was supported by the National Natural Science Foundation of China (No. 21925401) and the Natural Science Foundation of Hunan Province, China (No. 2020JJ4173).

References

[1] Brito, H. F.; Holsa, J.; Laamanen, T.; Lastusaari, M.; Malkamaki, M.; Rodrigues, L. C. V. Persistent luminescence mechanisms: human imagination at work. *Opt. Mater. Express* **2012**, *2*, 371–381.
[2] Du, J.; De Clercq, O. Q.; Poelman, D. Temperature dependent persistent luminescence: Evaluating the optimum working temperature. *Sci. Rep.* **2019**, *9*, 10517.
[3] Kabe, R.; Adachi, C. Organic long persistent luminescence. *Nature* **2017**, *550*, 384–387.
[4] Xu, J.; Ueda, J.; Tanabe, S. Toward tunable and bright deep-red per-

sistent luminescence of Cr^{3+} in garnets. *J. Am. Ceram. Soc.* **2017**, *100*, 4033–4044.
[5] Aitasalo, T.; Dereń, P.; Hölsä, J.; Jungner, H.; Krupa, J. C.; Lastusaari, M.; Legendziewicz, J.; Niittykoski, J.; Stręk, W. Persistent luminescence phenomena in materials doped with rare earth ions. *J. Solid State Chem.* **2003**, *171*, 114–122.
[6] Finley, E.; Brgoch, J. Deciphering the loss of persistent red luminescence in $ZnGa_2O_4$:Cr^{3+} upon Al^{3+} substitution. *J. Mater. Chem. C* **2019**, *7*, 2005–2013.
[7] Pan, Z.; Lu, Y. Y.; Liu, F. Sunlight-activated long-persistent luminescence in the near-infrared from Cr^{3+}-doped zinc gallogermanates. *Nat. Mater.* **2011**, *11*, 58–63.
[8] Finley, E.; Mansouri Tehrani, A.; Brgoch, J. Intrinsic Defects Drive Persistent Luminescence in Monoclinic $SrAl_2O_4$:Eu^{2+}. *J. Phys. Chem. C* **2018**, *122*, 16309–16314.
[9] Hu, G.; Cai, X.; Rong, Y. Crystal defects. In *Material Science*, De Gruyter, **2021**, pp 129–185.
[10] Huang, B. Native Point Defects in CaS: Focus on Intrinsic Defects and Rare Earth Ion Dopant Levels for Up-converted Persistent Luminescence. *Inorg. Chem.* **2015**, *54*, 11423–11440.
[11] Liu, F.; Yan, W.; Chuang, Y. J.; Zhen, Z.; Xie, J.; Pan, Z. Photostimulated near-infrared persistent luminescence as a new optical read-out from Cr^{3+}-doped $LiGa_5O_8$. *Sci. Rep.* **2013**, *3*, 1554.
[12] Maldiney, T.; Bessiere, A.; Seguin, J.; Teston, E.; Sharma, S. K.; Viana, B.; Bos, A. J.; Dorenbos, P.; Bessodes, M.; Gourier, D.; Scherman, D.; Richard, C. The *in vivo* activation of persistent nanophosphors for optical imaging of vascularization, tumours and grafted cells. *Nat. Mater.* **2014**, *13*, 418–426.
[13] Li, Y.; Gecevicius, M.; Qiu, J. Long persistent phosphors—from fundamentals to applications. *Chem. Soc. Rev.* **2016**, *45*, 2090–2136.
[14] Miao, S.; Xia, Z.; Molokeev, M. S.; Chen, M.; Zhang, J.; Liu, Q. Effect of Al/Si substitution on the structure and luminescence properties of $CaSrSiO_4$:Ce^{3+} phosphors: analysis based on the polyhedra distortion. *J. Mater. Chem. C* **2015**, *3*, 4616–4622.
[15] Lin, Y. H.; Zhang, Z. T.; Zhang, F.; Tang, Z. L.; Chen, Q. M. Preparation of the ultrafine SrAl2O4 : Eu,Dy needle-like phosphor and its optical properties. *Mater. Chem. Phys.* **2000**, *65*, 103–106.
[16] Ji, H.; Xie, G.; Lv, Y.; Lu, H. A new phosphor with flower-like structure and luminescent properties of $Sr_2MgSi_2O_7$:Eu^{2+}, Dy^{3+} long afterglow materials by sol–gel method. *J. Sol-Gel Sci. Technol.* **2007**, *44*, 133–137.
[17] Wu, S.; Pan, Z.; Chen, R.; Liu, X. *Long Afterglow Phosphorescent Materials*, Springer, **2017**.
[18] Dai, W. B. Investigation of the luminescent properties of Ce^{3+} doped and Ce^{3+}/Mn^{2+} co-doped $CaAl_2Si_2O_8$ phosphors. *RSC Adv.* **2014**, *4*, 11206–11215.
[19] Liu, N.; Chen, X.; Sun, X.; Sun, X.; Shi, J. Persistent luminescence nanoparticles for cancer theranostics application. *J. Nanobiotechnol.* **2021**, *19*, 1–24.
[20] Wu, S.; Li, Y.; Ding, W.; Xu, L.; Ma, Y.; Zhang, L. Recent Advances of Persistent Luminescence Nanoparticles in Bioapplications. *Nano-Micro Lett.* **2020**, *12*, 1–26.
[21] Buryakina, T. Y.; Su, P. T.; Syu, W., Jr.; Chang, C. A.; Fan, H. F.; Kao, F. J. Metabolism of HeLa cells revealed through autofluorescence lifetime upon infection with enterohemorrhagic Escherichia coli. *J. Biomed. Opt.* **2012**, *17*, 101503.
[22] Nakashima, N.; Yoshihara, K.; Tanaka, F.; Yagi, K. Picosecond fluorescence lifetime of the coenzyme of *D*-amino acid oxidase. *J. Biol. Chem.* **1980**, *255*, 5261–5263.
[23] Abdukayum, A.; Chen, J. T.; Zhao, Q.; Yan, X. P. Functional near infrared-emitting Cr^{3+}/Pr^{3+} co-doped zinc gallogermanate persistent luminescent nanoparticles with superlong afterglow for in vivo targeted bioimaging. *J. Am. Chem. Soc.* **2013**, *135*, 14125–14133.
[24] Wu, B. Y.; Wang, H. F.; Chen, J. T.; Yan, X. P. Fluorescence resonance energy transfer inhibition assay for alpha-fetoprotein excreted during cancer cell growth using functionalized persistent luminescence nanoparticles. *J. Am. Chem. Soc.* **2011**, *133*, 686–688.
[25] Liang, L.; Chen, N.; Jia, Y.; Ma, Q.; Wang, J.; Yuan, Q.; Tan, W. Recent progress in engineering near-infrared persistent luminescence nanoprobes for time-resolved biosensing/bioimaging. *Nano Res.* **2019**, *12*, 1279–1292.
[26] Ma, Q.; Wang, J.; Li, Z.; Lv, X.; Liang, L.; Yuan, Q. Recent Progress in Time-Resolved Biosensing and Bioimaging Based on Lanthanide-Doped Nanoparticles. *Small* **2019**, *15*, e1804969.
[27] Fan, W.; Lu, N.; Xu, C.; Liu, Y.; Lin, J.; Wang, S.; Shen, Z.; Yang, Z.; Qu, J.; Wang, T.; Chen, S.; Huang, P.; Chen, X. Enhanced Afterglow Performance of Persistent Luminescence Implants for Efficient Repeatable Photodynamic Therapy. *ACS Nano* **2017**, *11*, 5864–5872.
[28] Hai, O.; Yang, E.; Ren, Q.; Wu, X.; Ren, Y.; Zhao, Y.; Zhu, J. Enhancement of the persistent luminescence of $Sr_2MgSi_2O_7$:Eu^{2+},Dy^{3+} by Cu nanoparticles. *J. Lumin.* **2020**, *220*, 116965.
[29] Qu, B.; Wang, J.; Liu, K.; Zhou, R.; Wang, L. A comprehensive study of the red persistent luminescence mechanism of Y_2O_2S:Eu,Ti,Mg. *Phys. Chem. Chem. Phys.* **2019**, *21*, 25118–25125.
[30] Shi, J.; Sun, X.; Zhu, J.; Li, J.; Zhang, H. One-step synthesis of amino-functionalized ultrasmall near infrared-emitting persistent luminescent nanoparticles for *in vitro* and *in vivo* bioimaging. *Nanoscale* **2016**, *8*, 9798–9804.
[31] Song, L.; Lin, X. H.; Song, X. R.; Chen, S.; Chen, X. F.; Li, J.; Yang, H. H. Repeatable deep-tissue activation of persistent luminescent nanoparticles by soft X-ray for high sensitivity long-term in vivo bioimaging. *Nanoscale* **2017**, *9*, 2718–2722.
[32] Sun, S. K.; Wang, H. F.; Yan, X. P. Engineering Persistent Luminescence Nanoparticles for Biological Applications: From Biosensing/Bioimaging to Theranostics. *Acc. Chem. Res.* **2018**, *51*, 1131–1143.
[33] Wang, J.; Ma, Q.; Wang, Y.; Shen, H.; Yuan, Q. Recent progress in biomedical applications of persistent luminescence nanoparticles. *Nanoscale* **2017**, *9*, 6204–6218.
[34] Lecuyer, T.; Teston, E.; Ramirez-Garcia, G.; Maldiney, T.; Viana, B.; Seguin, J.; Mignet, N.; Scherman, D.; Richard, C. Chemically engineered persistent luminescence nanoprobes for bioimaging. *Theranostics* **2016**, *6*, 2488–2524.
[35] Luo, Q.; Wang, W.; Tan, J.; Yuan, Q. Surface Modified Persistent Luminescence Probes for Biosensing and Bioimaging: A Review. *Chin. J. Chem* . **2021**, *39*, 1009–1021.
[36] Li, Y. J.; Yan, X. P. Synthesis of functionalized triple-doped zinc gallogermanate nanoparticles with superlong near-infrared persistent luminescence for long-term orally administrated bioimaging. *Nanoscale* **2016**, *8*, 14965–14970.
[37] Wang, Y.; Yang, C. X.; Yan, X. P. Hydrothermal and biomineralization synthesis of a dual-modal nanoprobe for targeted near-infrared persistent luminescence and magnetic resonance imaging. *Nanoscale* **2017**, *9*, 9049–9055.
[38] Li, Z.; Zhang, Y.; Wu, X.; Huang, L.; Li, D.; Fan, W.; Han, G. Direct Aqueous-Phase Synthesis of Sub-10 nm "Luminous Pearls" with Enhanced *in Vivo* Renewable Near-Infrared Persistent Luminescence. *J. Am. Chem. Soc.* **2015**, *137*, 5304–5307.
[39] Qin, X.; Wang, J.; Yuan, Q. Synthesis and Biomedical Applications of Lanthanides-Doped Persistent Luminescence Phosphors with NIR Emissions. *Front. Chem.* **2020**, *8*, 608578.
[40] Tan, H.; Wang, T.; Shao, Y.; Yu, C.; Hu, L. Crucial Breakthrough of Functional Persistent Luminescence Materials for Biomedical and Information Technological Applications. *Front. Chem.* **2019**, *7*, 387.
[41] Zhou, Z.; Zheng, W.; Kong, J.; Liu, Y.; Huang, P.; Zhou, S.; Chen, Z.; Shi, J.; Chen, X. Rechargeable and LED-activated $ZnGa_2O_4$: Cr^{3+} near-infrared persistent luminescence nanoprobes for background-free biodetection. *Nanoscale* **2017**, *9*, 6846–6853.
[42] Hu, S.; Li, Z.; Luo, Q.; Ma, Q.; Chen, N.; Fu, L.; Wang, J.; Yang, R.; Yuan, Q. Facile Synthesis of Luminous Nanoparticles with Tunable Size and Long-Lived Luminescence for Lifetime-Based Biosensing. *Cryst. Growth Des.* **2019**, *19*, 2322–2328.
[43] Wang, J.; Ma, Q.; Hu, X. X.; Liu, H.; Zheng, W.; Chen, X.; Yuan, Q.; Tan, W. Autofluorescence-Free Targeted Tumor Imaging Based on Luminous Nanoparticles with Composition-Dependent Size and Persistent

Luminescence. *ACS Nano* **2017**, *11*, 8010–8017.
[44] Wang, J.; Ma, Q.; Zheng, W.; Liu, H.; Yin, C.; Wang, F.; Chen, X.; Yuan, Q.; Tan, W. One-Dimensional Luminous Nanorods Featuring Tunable Persistent Luminescence for Autofluorescence-Free Biosensing. *ACS Nano* **2017**, *11*, 8185–8191.
[45] Li, Z.; Wang, J.; Shen, R.; Chen, N.; Qin, X.; Wang, W.; Yuan, Q. Topological Radiated Dendrites Featuring Persistent Bactericidal Activity for Daily Personal Protection. *Small* **2021**, e2100562.
[46] Liu, H.; Hu, X.; Wang, J.; Liu, M.; Wei, W.; Yuan, Q. Direct low-temperature synthesis of ultralong persistent luminescence nanobelts based on a biphasic solution-chemical reaction. *Chin. Chem. Lett.* **2018**, *29*, 1641–1644.
[47] Hacaloğlu, J.; Uyar, T.; Ishida, H. Chapter 14 - Thermal Degradation Mechanisms of Polybenzoxazines. In *Handbook of Benzoxazine Resins*, Eds.: Ishida, H.; Agag, T., Elsevier, Amsterdam, **2011**, pp. 287–305.
[48] Ubaldini, A.; Artini, C.; Costa, G. A.; Carnasciali, M. M.; Masini, R. Synthesis and thermal decomposition of mixed GD-ND oxalates. *J. Therm. Anal. Calorim.* **2008**, *91*, 797–803.
[49] Hyeon, T.; Lee, S. S.; Park, J.; Chung, Y.; Bin Na, H. Synthesis of highly crystalline and monodisperse maghemite nanocrystallites without a size-selection process. *J. Am. Chem. Soc.* **2001**, *123*, 12798–12801.
[50] Salavati-Niasari, M.; Davar, F.; Mazaheri, M. Synthesis of Mn_3O_4 nanoparticles by thermal decomposition of a [bis(salicylidiminato)-manganese(II)] complex. *Polyhedron* **2008**, *27*, 3467–3471.
[51] Lassenberger, A.; Grunewald, T. A.; van Oostrum, P. D. J.; Rennhofer, H.; Amenitsch, H.; Zirbs, R.; Lichtenegger, H. C.; Reimhult, E. Monodisperse Iron Oxide Nanoparticles by Thermal Decomposition: Elucidating Particle Formation by Second-Resolved in Situ Small-Angle X-ray Scattering. *Chem. Mater.* **2017**, *29*, 4511–4522.
[52] Hyeon, T. Chemical synthesis of magnetic nanoparticles. *Chem. Commun.* **2003**, 927–934.
[53] Lu, A. H.; Salabas, E. L.; Schuth, F. Magnetic nanoparticles: synthesis, protection, functionalization, and application. *Angew. Chem. Int. Ed.* **2007**, *46*, 1222–1244.
[54] Odularu, A. T. Metal Nanoparticles: Thermal Decomposition, Biomedicinal Applications to Cancer Treatment, and Future Perspectives. *Bioinorg. Chem. Appl.* **2018**, *2018*, 9354708.
[55] Lv, X.; Chen, N.; Wang, J.; Yuan, Q. Facile thermal decomposition synthesis of sub-5 nm nanodots with long-lived luminescence for autofluorescence-free bioimaging. *Sci. China Mater.* **2020**, *63*, 1808–1817.
[56] Sun, X.; Song, L.; Liu, N.; Shi, J.; Zhang, Y. Chromium-Doped Zinc Gallate Near-Infrared Persistent Luminescence Nanoparticles in Autofluorescence-Free Biosensing and Bioimaging: A Review. *ACS Appl. Nano Mater.* **2021**, *4*, 6497–6514.
[57] Mondal, A.; Das, S.; Manam, J. Hydrothermal synthesis, structural and luminescent properties of a Cr^{3+} doped $MgGa_2O_4$ near-infrared long lasting nanophospor. *RSC Adv.* **2016**, *6*, 82484–82495.
[58] Zhou, Z.; Li, Y.; Peng, M. Near-infrared persistent phosphors: Synthesis, design, and applications. *Chem. Eng. J.* **2020**, *399*, 125688.
[59] Shi, J.; Sun, X.; Zheng, S.; Li, J.; Fu, X.; Zhang, H. A new near-infrared persistent luminescence nanoparticle as a multifunctional nanoplatform for multimodal imaging and cancer therapy. *Biomaterials* **2018**, *152*, 15–23.
[60] Ran, C.; Zhang, Z.; Hooker, J.; Moore, A. In vivo photoactivation without "light": use of Cherenkov radiation to overcome the penetration limit of light. *Mol. Imaging Biol.* **2012**, *14*, 156–162.
[61] Fu, L.; Wang, J.; Chen, N.; Ma, Q.; Lu, D.; Yuan, Q. Enhancement of long-lived luminescence in nanophosphors by surface defect passivation. *Chem. Commun.* **2020**, *56*, 6660–6663.
[62] Deng, R.; Qin, F.; Chen, R.; Huang, W.; Hong, M.; Liu, X. Temporal full-colour tuning through non-steady-state upconversion. *Nat. Nanotechnol.* **2015**, *10*, 237–242.
[63] Zheng, W.; Zhou, S.; Chen, Z.; Hu, P.; Liu, Y.; Tu, D.; Zhu, H.; Li, R.; Huang, M.; Chen, X. Sub-10 nm lanthanide-doped CaF_2 nanoprobes for time-resolved luminescent biodetection. *Angew. Chem. Int. Ed.* **2013**, *52*, 6671–6676.
[64] Ma, Q.; Wang, J.; Zheng, W.; Wang, Q.; Li, Z.; Cong, H.; Liu, H.; Chen, X.; Yuan, Q. Controlling disorder in host lattice by hetero-valence ion doping to manipulate luminescence in spinel solid solution phosphors. *Sci. China Mater.* **2018**, *61*, 1624–1629.
[65] Sundaresan, A.; Rao, C. N. R. Ferromagnetism as a universal feature of inorganic nanoparticles. *Nano Today* **2009**, *4*, 96–106.
[66] Xiong, J.; Di, J.; Li, H. Charge steering in ultrathin 2D nanomaterials for photocatalysis. *J. Mater. Chem. A* **2020**, *8*, 12928–12950.
[67] Zhou, W.; Fu, H. Defect-mediated electron–hole separation in semiconductor photocatalysis. *Inorg. Chem. Front.* **2018**, *5*, 1240–1254.
[68] Mao, J.; Chen, Y.; Pei, J.; Wang, D.; Li, Y. Pt-M (M = Cu, Fe, Zn, etc.) bimetallic nanomaterials with abundant surface defects and robust catalytic properties. *Chem. Commun.* **2016**, *52*, 5985–5988.
[69] Xiong, J.; Di, J.; Xia, J.; Zhu, W.; Li, H. Surface Defect Engineering in 2D Nanomaterials for Photocatalysis. *Adv. Funct. Mater.* **2018**, *28*, 1801983.
[70] Pei, P.; Chen, Y.; Sun, C.; Fan, Y.; Yang, Y.; Liu, X.; Lu, L.; Zhao, M.; Zhang, H.; Zhao, D.; Liu, X.; Zhang, F. X-ray-activated persistent luminescence nanomaterials for NIR-II imaging. *Nat. Nanotechnol.* **2021**, DOI: 10.1038/s41565-021-00922-3.
[71] Hu, H.; Zhang, W. Synthesis and properties of transition metals and rare-earth metals doped ZnS nanoparticles. *Opt. Mater.* **2006**, *28*, 536–550.
[72] Prakash, J.; Samriti; Kumar, A.; Dai, H.; Janegitz, B. C.; Krishnan, V.; Swart, H. C.; Sun, S. Novel rare earth metal–doped one-dimensional TiO_2 nanostructures: Fundamentals and multifunctional applications. *Mater. Today Sustainability* **2021**, *13*, 100066.
[73] Yang, Y.; Zhang, F. Activatable Chemiluminescent Molecular Probes for Bioimaging and Biosensing. *Anal. Sens.* **2021**, *1*, 75–89.
[74] Adeel, M.; Rahman, M. M.; Caligiuri, I.; Canzonieri, V.; Rizzolio, F.; Daniele, S. Recent advances of electrochemical and optical enzyme-free glucose sensors operating at physiological conditions. *Biosens. Bioelectron.* **2020**, *165*, 112331.
[75] Drummen, G. P. Fluorescent probes and fluorescence (microscopy) techniques--illuminating biological and biomedical research. *Molecules* **2012**, *17*, 14067–14090.
[76] Liu, W.; Chen, J.; Xu, Z. Fluorescent probes for biothiols based on metal complex. *Coord. Chem. Rev.* **2021**, *429*, 213638.
[77] Liu, H.; Li, Z.; Shen, R.; Li, Z.; Yang, Y.; Yuan, Q. Point-of-Care Pathogen Testing Using Photonic Crystals and Machine Vision for Diagnosis of Urinary Tract Infections. *Nano Lett.* **2021**, *21*, 2854–2860.
[78] Wang, J.; Ma, Q.; Liu, H.; Wang, Y.; Shen, H.; Hu, X.; Ma, C.; Yuan, Q.; Tan, W. Time-Gated Imaging of Latent Fingerprints and Specific Visualization of Protein Secretions via Molecular Recognition. *Anal. Chem.* **2017**, *89*, 12764–12770.
[79] Wang, Y.; Li, Z.; Lin, Q.; Wei, Y.; Wang, J.; Li, Y.; Yang, R.; Yuan, Q. Highly Sensitive Detection of Bladder Cancer-Related miRNA in Urine Using Time-Gated Luminescent Biochip. *ACS Sens.* **2019**, *4*, 2124–2130.
[80] Yoon, S.; Feng, J.; Jain, A. K. Altered fingerprints: analysis and detection. *IEEE Trans. Pattern Anal. Mach. Intell.* **2012**, *34*, 451–464.
[81] Widjaja, E. Latent fingerprints analysis using tape-lift, Raman microscopy, and multivariate data analysis methods. *Analyst* **2009**, *134*, 769–775.
[82] Seah, L. K.; Dinish, U. S.; Phang, W. F.; Chao, Z. X.; Murukeshan, V. M. Fluorescence optimisation and lifetime studies of fingerprints treated with magnetic powders. *Forensic Sci. Int.* **2005**, *152*, 249–257.
[83] Li, Z.; Wang, Q.; Wang, Y.; Ma, Q.; Wang, J.; Li, Z.; Li, Y.; Lv, X.; Wei, W.; Chen, L.; Yuan, Q. Background-free latent fingerprint imaging based on nanocrystals with long-lived luminescence and pH-guided recognition. *Nano Res.* **2018**, *11*, 6167–6176.
[84] Vigneshvar, S.; Sudhakumari, C. C.; Senthilkumaran, B.; Prakash, H. Recent Advances in Biosensor Technology for Potential Applications - An Overview. *Front. Bioeng. Biotechnol.* **2016**, *4*, 11.
[85] Zhou, J.; Liu, Z.; Li, F. Upconversion nanophosphors for small-animal imaging. *Chem. Soc. Rev.* **2012**, *41*, 1323–1349.

[86] Dasari, S.; Wudayagiri, R.; Valluru, L. Cervical cancer: Biomarkers for diagnosis and treatment. *Clin. Chim. Acta* **2015**, *445*, 7–11.
[87] Xu, L. P.; Chen, Y.; Yang, G.; Shi, W.; Dai, B.; Li, G.; Cao, Y.; Wen, Y.; Zhang, X.; Wang, S. Ultratrace DNA Detection Based on the Condensing-Enrichment Effect of Superwettable Microchips. *Adv. Mater.* **2015**, *27*, 6878–6884.
[88] Cui, L.; Zou, Y.; Lin, N.; Zhu, Z.; Jenkins, G.; Yang, C. J. Mass amplifying probe for sensitive fluorescence anisotropy detection of small molecules in complex biological samples. *Anal. Chem.* **2012**, *84*, 5535–5541.
[89] Vo-Dinh, T.; Cullum, B. M.; Stokes, D. L. Nanosensors and biochips: frontiers in biomolecular diagnostics. *Sens. Actuators, B* **2001**, *74*, 2–11.

Manuscript received: May 29, 2021
Manuscript revised: July 26, 2021
Manuscript accepted: August 7, 2021
Accepted manuscript online: August 10, 2021

